International Journal of Heat and Mass Transfer 135 (2019) 460–469

Contents lists available at ScienceDirect

International Journal of Heat and Mass Transfer

journal homepage: www.elsevier.com/locate/ijhmt

A two-dimensional model for the design of flow fields in vanadium redox flow batteries

B.W. Zhang [a], Y. Lei [a], B.F. Bai [a], T.S. Zhao [b,*]

[a] State Key Laboratory of Multiphase Flow in Power Engineering, Xi'an Jiaotong University, Xi'an 710049, China
[b] HKUST Energy Institute, Department of Mechanical and Aerospace Engineering, The Hong Kong University of Science and Technology, Hong Kong, China

ARTICLE INFO

Article history:
Received 26 October 2018
Received in revised form 2 February 2019
Accepted 3 February 2019
Available online 10 February 2019

Keywords:
Vanadium redox flow battery
Design of flow field
Two-dimensional mathematical model

ABSTRACT

In this work, we report a two-dimensional mathematical model for the design of flow fields in vanadium redox flow batteries (VRFBs). The model is validated by calculating the pressure drop, distribution uniformity of vanadium ions in an interdigitated flow field and a serpentine flow field for a 9-cm^2 cell. The model is then used to simulate interdigitated and a series of parallel serpentine design of flow fields in a 410-cm^2 cell. It is demonstrated that with an increase in the number of parallel serpentine channels, the pumping power decreases while the distribution of vanadium ions becomes less uniform. Among the design of flow fields studied in this work, the interdigitated design performs the lowest pumping power and the most uniform distributions of vanadium ions.

© 2019 Elsevier Ltd. All rights reserved.

1. Introduction

As a promising electrochemical energy storage system, VRFBs demonstrate much attraction for smoothing output of intermittent power plants, such as wind and solar power sources [1–6]. Its distinctive features such as decoupling of power and capacity, elimination of crossover contamination and long cycle life arouse the rapid development of VRFBs. However, high cost of stack and electrolyte hinder its commercialization. In a typical stack of traditional flow-through type battery, thick porous electrode is usually utilized to decrease the electrolyte velocity, aiming to lower the pressure drop associated with pumping power loss. Herein, limiting current density of VRFB cell is usually very low because of large electric resistance. Compared with traditional flow-through type battery, the application of flow fields caved with channels reduces the thickness of porous electrode with low pressure drop guaranteed. Thus, Ohmic polarization is dramatically reduced and high limiting current density is achieved. The cell size could be miniaturized with the application of high current density for a rated power. As a result, the material costs of stack composition are lowered consequently. However, when larger size cell is required for the scale-up of stack and commercialization of VRFB system, the inadequate mass transport compared with flow batteries without flow field hinders the optimization of performance seriously. Therefore, the improvement of uniformity becomes a key issue in the VRFB with flow field.

Considering that flow field types and specification parameters are the essential factors determining the uniformity of electrolyte, designs of carved channels in bipolar plates influence the battery performance significantly, especially at different operation conditions. The flow field design contributes much to mass transport in porous electrodes. We need to propose appropriate flow field design to provide reactants uniformly in the porous electrodes. Initially applied in fuel cells, numerous types of flow fields have been proposed in VRFBs, such as parallel, serpentine, interdigitated and multi serpentine designs [7–13]. In these design of flow fields, electrolyte is pumped from the reservoirs into the stack cells flows through the caved channels and distributed into the porous electrodes. Due to the electrochemical reactions in porous electrodes, reactant concentrations vary along with the electrolyte flow in cells. Thus, design of flow fields influence the convective mass transport, leading to significant effects on vanadium ion concentrations.

Numerous flow field designs have been put forward for VRFBs in experimental studies. Serpentine flow field design was introduced with several layers of carbon paper applied as porous electrodes [14]. This study revealed that this architecture could dramatically reduce the Ohmic resistances, resulting in much better battery performance. With the increase of carbon paper layers, electrochemical active area grew proportionally. Herein, the number of carbon paper layers also needed to be carefully designed. Dennison and co-workers [15] studied the effect of flow field

* Corresponding author.
E-mail address: metzhao@ust.hk (T.S. Zhao).

https://doi.org/10.1016/j.ijheatmasstransfer.2019.02.008
0017-9310/© 2019 Elsevier Ltd. All rights reserved.

Nomenclature

A	area, m^2
a	specific surface area, m^{-1}
c	concentration, $mol \cdot m^{-3}$
D	diffusion coefficient, $m^2 \cdot s^{-1}$
d	thickness, m
E	potential, V
F	Faraday constant, $C \cdot mol^{-1}$
k	reaction rate constant, $m \cdot s^{-1}$
p	pressure, Pa
P	power, W
R	gas constant, $J \cdot mol^{-1} \cdot K^{-3}$
S	mass source, $mol \cdot m^{-3}$
T	temperature, K
v	electrolyte flow velocity, $m \cdot s^{-1}$

Greek

α	charge transfer coefficient
ε	porosity
η	overpotential, V
μ	dynamic viscosity, Pa·s
ρ	density, $kg \cdot m^{-3}$
σ	conductivity, $S \cdot m^{-1}$
ϕ	potential, V
ω	flow rate, $m^3 \cdot s^{-1}$
κ	permeability, m^2
ψ	efficiency

Superscripts and subscripts

a	anodic
c	cathodic
mt	mass transfer coefficient
neg	negative side
pos	positive side
h	height
w	width
ref	reference value
I	region (I)
II	region (II)

design on mass transport. Four design of flow fields, namely serpentine, parallel, interdigitated and spiral designs were tested. The results revealed that the perforations in carbon paper electrodes with flow fields of serpentine, parallel and spiral designs enhanced the mass transport into porous electrodes. However, the perforations in carbon paper electrodes with flow fields of interdigitated design performed the negative influence. Herein, proper flow field designs need to be proposed considering the structure of porous electrodes. Houser et al. [16] compared the serpentine and interdigitated design of flow fields. Through numerical and experimental approaches, they inferred that the pressure drop and battery performance were influenced not only by design of flow fields, but also by porous electrode properties and operation conditions. Herein, it was hardly figured out the best flow field design for VRFBs. In a further study, Houser et al. [17] proposed several new types of design of flow fields and studied the performance and pressure drop at different operation conditions. It was concluded that the new proposed aspect ratio design demonstrated much improvement of battery performance with little increasing in pressure drop. Marschewski et al. [18] fabricated networks flow field with 3-D print technology. This flow field design combined the heat management with elevated mass transport in flow battery, exploring increasing in overall efficiency of VRFBs.

Other than the experimental studies demonstrated above, numerical simulation has been widely utilized in the investigation of transport phenomena and flow field design in vanadium redox flow batteries [19–35]. Employed with a two dimensional model describing the mass, charge, momentum transport and conservation coupled with electrochemical kinetics for vanadium ions, Shah et al. [19] investigated the effects of vanadium ions concentration, flow rates and electrode porosity on battery performance in a flow through type VRFB. Based on this developed model, Shah and coworkers [20,21] further carried out the studies on effects of side reactions such as hydrogen and oxygen evolution in VRFB. To derive the solutions rapidly and accurately for controlling and monitoring in VRFB, Shah et al. [22] developed a dynamic analytical model involving the transport processes coupled with electrochemical kinetics. Knehr et al. [23] considered the effect of concentration of hydrogen ion and also the Donnan effect across membrane to develop a more reasonable model for vanadium redox flow batteries. With this model, the open circuit voltage in simulation can meet the measured data very well. Coupling the transport processes in porous electrodes, electrolyte and membrane, Knehr et al. [24] proposed a transient two dimensional model for vanadium redox flow batteries with species crossover through membrane considered. You et al. [25] developed a coupling model for the simplification of mathematical description in fluid flow, ions and charge transport and also the electrochemical reactions. Considering the self-discharge process derived from the crossover of vanadium ions through membrane, You et al. [26] presented a simple mathematic model for a kilowatt-class VRFB stack. The diffusion rate of vanadium ions across membrane were determined. Ke et al. [27,28] developed an analytical model for a vanadium redox flow batteries with serpentine flow fields. The model was capable to determine the key influencing factors on flow penetration into the porous electrodes and limiting current densities. Based on two and three dimensional models for electrolyte flow in layered serpentine channel over porous electrode in VRFB, Ke et al. [29,30] examined the electrolyte penetration into porous electrodes and the effect on battery performance. Ye et al. [31] investigated the system trade-off optimization between efficiency and through the analog circuit and flow network model for a multi-stack VRFB. The shunt current and pumping loss in a multi stacks are examined. You et al. [32] studied the design optimization for interdigitated flow field. Xu et al. [33] compared the battery performance of VRFB without flow field and that with serpentine and parallel flow fields. They concluded that serpentine flow field design was more suitable for VRFB concerning battery performance and pump power consumption associated with pressure drop. Knudsen et al. [34] numerically investigated the electrolyte flow and pressure drop in wide range of design of flow fields with porous electrodes. The results showed that pressure drop and electrolyte distribution were significantly influenced by design of flow fields for various area cells. Messaggi et al. [35] investigated the influence of serpentine and interdigitated design of flow fields on the performance of a 25-cm^2 VRFB. It was demonstrated that serpentine flow field design showed better performance that interdigitated flow field design at all the operation conditions in their study.

In a medium/large-scale VRFB system, electrolyte pumped from the reservoirs is distributed into cells through flow frame, then flows in the designed flow fields and porous electrodes. Electro-

chemical reactions occur at the surface of carbon fibers when electrolyte flows through porous electrode. Due to the large-scale difference between in-plane and through-plane directions in flow fields, usually hundreds of millimeters and several millimeters separately, the distribution of vanadium concentrations is mainly influenced by the convection mass transport and electrochemical reactions along the in-plane direction. To achieve reasonable trade-off between pressure drop associated with pump power consumption and uniformity of vanadium concentration distribution, the flow fields need to be carefully designed, typically with complex structures. Numerical simulation is a useful tool for the design of flow fields. However, the three-dimensional model needs much excessive computational consumption in these cases for flow field design, especially for a large size of flow field with series of configuration and operation parameters considered. Meanwhile, the details of fluid flow, mass transport coupled with electrochemical reactions in designed flow fields need to be carefully considered. Therefore, a two-dimensional model with adequate accuracy is suitable for the simulation of complex flow field design.

In this work, we report a two-dimensional model for fluid flow, mass transport coupled with electrochemical reaction kinetics in porous electrode for the design of flow fields in VRFBs. With appropriate indicators such as uniformity factors of current densities and vanadium ion concentration, the uniformity of reactants and electrochemical reactions distributions in VRFBs is investigated. Moreover, interdigitated and parallel serpentine flow fields are designed in an industrial-scale cell and the developed model is applied to evaluate the performance of these designs. Most of previous models concern little about the optimization of distribution uniformity in industrial-class cells, which is important for commercialization of VRFB. Our work is mainly focusing on the development of sufficient tools for flow field design with uniform distributions in industrial-class cells. The rest sections of this paper are constructed as follows. The governing equations and boundary conditions of mathematical model describing the fluid flow, mass transport coupled with electrochemical reactions are presented in Section 2. Moreover, the results and discussion on the pressure drop, distributions of current densities and electrolyte concentrations are demonstrated in Section 3. Finally, the conclusions are drawn in Section 4.

2. Mathematical model

The determination of channel specifications and parameters in design of flow fields plays a key role for the performance improvement. Through flow fields with channels carved, the electrolyte is distributed into porous electrodes where electrochemical reactions occur. The design of flow fields and porous electrode properties lead to different electrolyte flow patterns and distribution uniformity. Unlike previous traditional model with channel domain and porous electrode domain divided according to the geometric structures as described in literature [16], the computational domains of our model are divided into two regions (I) and (II) as shown in Fig. 1. To efficiently calculate the fluid flow in channels of flow field, the electrolyte flow in porous electrode under channels is neglected considering the large discrepancies of permeability between channels and porous electrodes. Concentrations of all species in porous electrodes under channels are reasonably assumed to be the same as that in channels and flow field design at positive side is considered in this work.

Continuity equation in both regions (I) and (II) is expressed as:

$$\rho\nabla\cdot\vec{v}=0 \tag{1}$$

Electrolyte flow in regions (I) and (II) are described by Navier-Stokes equation and Brinkman equation, separately:

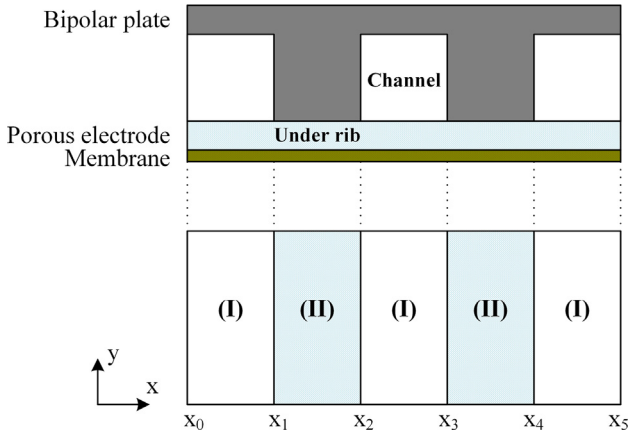

Fig. 1. Schematics of (upper) flow field structure and (bottom) computational regions.

$$\rho\left(\vec{v}\cdot\nabla\right)\vec{v}=\nabla\cdot\left[-pI+\mu\left(\nabla\vec{v}+\left(\nabla\vec{v}\right)^{T}\right)\right] \tag{2}$$

$$\frac{\rho}{\varepsilon^{2}}\left(\vec{v}\cdot\nabla\right)\vec{v}=\nabla\cdot\left[-pI+\frac{\mu}{\varepsilon}\left(\nabla\vec{v}+\left(\nabla\vec{v}\right)^{T}\right)\right]-\frac{\mu}{\kappa}\vec{v} \tag{3}$$

where ρ denotes the electrolyte density, ε denotes the porosity of carbon felt electrode, $\vec{v}$ denotes the velocity of electrolyte flow, μ denotes the viscosity, κ denotes the permeability in porous electrodes, which can be expressed through Kozeny-Carman equation by [36]:

$$\kappa=\frac{d_f^2\varepsilon^3}{16k_{CK}(1-\varepsilon)^2} \tag{4}$$

Due to the pressure gradients between adjacent flow channels, the electrolyte flow penetrates into the porous electrodes, resulting in the "by-passing" flow patterns in both serpentine and interdigitated flow field designs. At the interface between two regions such as $x=x_2$, mass flux of electrolyte in region (II) is expressed as:

$$\int\vec{J}_{m,II}\cdot\vec{n}\,\mathrm{d}z=\int\vec{J}_{m,I}\cdot\vec{n}\,\mathrm{d}z \tag{5}$$

where $\vec{J}_m$ denotes the mass flux, $\vec{n}$ denotes the direction vector perpendicular to the interfaces. The subscripts I and II denote the regions (I) and (II) respectively.

Velocity profile perpendicular to the interfaces is assumed as parabolic flow along the z direction, according to the literature [37]:

$$\left(\vec{v}_I\cdot\vec{n}\right)_{average}=\frac{2}{3}\vec{v}_I\cdot\vec{n} \tag{6}$$

Combined equation (5) and (6), the velocity at the interface between two regions (I) and (II) can be expressed as:

$$\vec{v}_{II}=\frac{2d_h\vec{v}_I\cdot\vec{n}}{3\varepsilon d_e} \tag{7}$$

where d_e denotes the electrode thickness, d_h denotes the channel height.

Conservation equations for the vanadium transport in region (I) are expressed by:

$$\nabla\cdot(-D_i\nabla c_i)+\vec{v}\cdot\nabla c_i=S_i \tag{8}$$

where D denotes the diffusion coefficient, c denotes the vanadium concentration and $\vec{v}$ is the electrolyte velocity. The subscript i ($i=2,\ 3,\ 4,\ 5$) denotes the V^{2+}, V^{3+}, VO^{2+} and VO_2^+ vanadium ions.

S are equivalent species sources and expressed as $ai_{local}d_e/d_h$ and $-ai_{local}d_e/d_h$ for vanadium ions V^{2+} and V^{3+} at negative side, and $ai_{local}d_e/d_h$ and $-ai_{local}d_e/d_h$ for vanadium ions VO^{2+} and VO_2^+ at positive side. d_e denotes porous electrode thickness, d_h denotes channel height, i_{local} denotes the local current density at surface of carbon fibers, and a denotes the specific surface area of porous electrodes, which can be calculated by [38]:

$$a = \frac{4(1-\varepsilon)}{d_f} \tag{9}$$

Conservation equations describing the vanadium transport processes in region (II) are expressed by:

$$\nabla \cdot \left(-\varepsilon^{3/2} D_i \nabla c_i\right) + \vec{v} \cdot \nabla c_i = S_i \tag{10}$$

where S denotes the sources of vanadium ions, which are expressed as ai_{local} and $-ai_{local}$ for vanadium ions V^{2+} and V^{3+} at negative side, and ai_{local} and $-ai_{local}$ for vanadium ions VO^{2+} and VO_2^+.

At the interface between regions (I) and (II) such as $x = x_2$, vanadium ion concentrations are identical:

$$c_{II} = c_I \tag{11}$$

After transporting from the flow field channels, electrochemical reactions occurred at the surface of carbon fibers in porous electrodes. Sources of vanadium ions are related to local current densities. Local current density at the surface of carbon fibers is described by Butler-Volmer equation at negative and positive sides are expressed respectively as:

$$\begin{aligned} i_{local,neg} &= i^0_{neg}\left(\exp\left(\alpha_{c,neg}\eta_{neg}F/RT\right) - \exp\left(-\alpha_{a,neg}\eta_{neg}F/RT\right)\right) \\ i_{local,pos} &= i^0_{pos}\left(\exp\left(\alpha_{c,pos}\eta_{pos}F/RT\right) - \exp\left(-\alpha_{a,pos}\eta_{pos}F/RT\right)\right) \end{aligned} \tag{12}$$

where F denotes Faraday constant, R denotes gas constant, T denotes temperature, α denotes the charge transfer coefficients, which are 0.5 in this work. The subscripts a and c denote anodic and cathodic respectively.

The exchange current density of positive electrochemical reactions is described by:

$$\begin{aligned} i^0_{neg} &= Fk_{neg}\left(c^s_2\right)^{\alpha_{a,neg}}\left(c^s_3\right)^{\alpha_{c,neg}} \\ i^0_{pos} &= Fk_{pos}\left(c^s_4\right)^{\alpha_{a,pos}}\left(c^s_5\right)^{\alpha_{c,pos}} \end{aligned} \tag{13}$$

where k is electrochemical reaction rate constant and the superscript s denotes the surface of carbon fibers.

Over potential at positive side is calculated via:

$$\begin{aligned} \eta_{neg} &= E_{neg} - \left(E^0_{neg} + \tfrac{RT}{F}\ln\tfrac{c_3}{c_2}\right) - r_{neg}i_{applied,neg} \\ \eta_{pos} &= E_{pos} - \left(E^0_{pos} + \tfrac{RT}{F}\ln\left(\tfrac{c_5\left(c_{H^+}/c^{ref}\right)^2}{c_4}\right)\right) - r_{pos}i_{applied,pos} \end{aligned} \tag{14}$$

where r_{neg} and r_{pos} denotes the areal resistance of negative and positive porous electrodes, respectively. T denotes the temperature.

Current density distribution is calculated from local current density by:

$$\begin{aligned} i_{applied,neg} &= ad_e i_{local,neg} \\ i_{applied,pos} &= ad_e i_{local,pos} \end{aligned} \tag{15}$$

where a denotes the specific area. Ohmic resistances are derived from conductivity of electrolyte associated with SOC of electrolyte:

$$\begin{aligned} r_{neg} &= \tfrac{d_e}{\varepsilon^{3/2}\sigma_{e,neg}} \\ r_{pos} &= \tfrac{d_e}{\varepsilon^{3/2}\sigma_{e,pos}} \end{aligned} \tag{16}$$

Conductivity of electrolyte is calculated from the electrolyte SOC according to the experimental correlation [39]:

$$\begin{aligned} \sigma_{e,neg} &= 7.699 \times SOC + 35.716(S/m) \\ \sigma_{e,pos} &= 12.251 \times SOC + 43.763(S/m) \end{aligned} \tag{17}$$

Combined with the experimental correlation describing local mass transfer process in porous electrodes, the vanadium concentrations at the surface of carbon fibers can be calculated. SOC of electrolyte flow changes slowly due to the relatively large electrolyte volume in reservoirs compared with electrolyte volume in cells. Therefore, the transport of vanadium ions at the surface of carbon fibers are reasonably regarded as quasi-equilibrium state. Concentrations of VO^{2+} and VO_2^+ are derived as:

$$c^s_2 = \frac{c_2 + k_{neg}\exp\left(-\frac{\eta_{neg}F}{2RT}\right)\left(\frac{c_2}{k^{mt}_3} + \frac{c_3}{k^{mt}_2}\right)}{1 + k_{neg}\left(\exp\left(-\frac{\eta_{neg}F}{2RT}\right)/k^{mt}_3 + \exp\left(\frac{\eta_{neg}F}{2RT}\right)/k^{mt}_2\right)} \tag{18}$$

$$c^s_3 = \frac{c_3 + k_{neg}\exp\left(\frac{\eta_{neg}F}{2RT}\right)\left(\frac{c_2}{k^{mt}_3} + \frac{c_3}{k^{mt}_2}\right)}{1 + k_{neg}\left(\exp\left(-\frac{\eta_{neg}F}{2RT}\right)/k^{mt}_3 + \exp\left(\frac{\eta_{neg}F}{2RT}\right)/k^{mt}_2\right)} \tag{19}$$

$$c^s_4 = \frac{c_4 + k_{pos}\exp\left(-\frac{\eta_{pos}F}{2RT}\right)\left(\frac{c_4}{k^{mt}_5} + \frac{c_5}{k^{mt}_4}\right)}{1 + k_{pos}\left(\exp\left(-\frac{\eta_{pos}F}{2RT}\right)/k^{mt}_5 + \exp\left(\frac{\eta_{pos}F}{2RT}\right)/k^{mt}_4\right)} \tag{20}$$

$$c^s_5 = \frac{c_5 + k_{pos}\exp\left(\frac{\eta_{pos}F}{2RT}\right)\left(\frac{c_4}{k^{mt}_5} + \frac{c_5}{k^{mt}_4}\right)}{1 + k_{pos}\left(\exp\left(-\frac{\eta_{pos}F}{2RT}\right)/k^{mt}_5 + \exp\left(\frac{\eta_{pos}F}{2RT}\right)/k^{mt}_4\right)} \tag{21}$$

Local mass transfer coefficients are calculated through:

$$k^{mt}_i = \frac{D_i}{\delta} \tag{22}$$

where δ denotes the average inter-fiber distance in porous electrodes.

Flow field structure influences the mass transport of vanadium ions in VRFBs. Along with the electrolyte flow, electrochemical reactions occurred with the consumption and production of vanadium ions, determining the vanadium concentrations in porous electrodes and channels. Herein, distribution uniformity across cells is of great significance in reflecting the fitness of flow field design. In this work, the uniformity factor is utilized to evaluate the uniformity of current density distribution and vanadium concentration distribution. The uniformity factors are introduced to describe the distribution uniformity of current density, V^{2+} and VO_2^+ [40]:

$$U_i = 1 - \frac{1}{i_m}\sqrt{\frac{1}{A}\iint (i - i_m)^2 \mathrm{d}A} \tag{23}$$

$$U_{V^{2+}} = 1 - \frac{1}{c_{2,m}}\sqrt{\frac{1}{A}\iint (c_2 - c_{2,m})^2 \mathrm{d}A} \tag{24}$$

$$U_{VO_2^+} = 1 - \frac{1}{c_{5,m}}\sqrt{\frac{1}{A}\iint (c_5 - c_{5,m})^2 \mathrm{d}A} \tag{25}$$

where A denotes the active membrane area. i denotes current density, c_2 and c_5 are concentrations of V^{2+} and VO_2^+, respectively. i_m, $c_{2,m}$ and $c_{5,m}$ are average values.

The boundary conditions are expressed as follows. At the inlet of flow fields, velocity is calculated as follows according to the literature which describes the velocity profile of developed laminar flow in rectangular ducts [41]:

$$v_{in} = 2.11\frac{\omega}{N_{channel}d_h d_w}\left(1 - (2x/d_w)^{2.2}\right) \tag{26}$$

where ω denotes the electrolyte flow rate, $N_{channel}$ denotes the parallel channel number and d_w denotes the channel width. The pressure at cell outlet is set as reference. Other boundaries except interface of regions are set to non-slip, solid and insulated walls.

The configurations and parameters in simulation are listed in Table 1 except parameters otherwise stated. Conservation equations for the fluid flow and mass transport coupled with electrochemical kinetics are computed with the non-linear solver PARDISO in Comsol Multiphysics. The fluid flow in channels and porous electrodes is described by the *Free and Porous Media Flow* option. The mass transport in electrolyte is described by the *Transport of Diluted Species* option. The equations associated with electrochemical kinetics are introduced through the self-written codes. The relative error was set to 10^{-6}.

3. Results and discussion

3.1. Model validation

To validate our developed model, a 9-cm^2 cell with serpentine and interdigitated flow fields were applied as shown in Fig. 2. The calculated design of flow field was identical to the channel structures in literature [16]. Height d_h and width d_w of channels are both 1 mm and single channel is applied in the serpentine flow field design.

We compare the simulation results of the three-dimensional and two-dimensional models with experimental data reported by Houser et al. [16]. As depicted in Fig. 3(a) and (b), the calculated pressure drop meets the experimental data very well for ranges of flow rates. More importantly, the simulation results reveal that two-dimensional model is of great agreement with three-dimensional model, indicating that the two-dimensional model is appropriate for pressure drop evaluation in flow field design. The pumped power consumption of serpentine flow field is much larger than that of interdigitated flow field. Regarding the electrolyte flow distributions in channels, flow paths from the inlet are relatively short and cross-sectional area is much larger in interdigitated flow field design than that in serpentine design of flow fields. Herein, electrolyte flow velocity is rather low in the interdigitated flow field channels at a certain flow rate, resulting in relatively low pressure drop compared with serpentine design of flow fields.

Table 1
Configurations and parameters in simulation.

Parameter	Value
Electrolyte viscosity [16], μ	3.237×10^{-3} Pa·s
Electrolyte density [16], ρ	1.5×10^{3} kg·m^{-3}
Uncompressed electrode thickness [16], d_e^0	4.1×10^{-4} m
Uncompressed electrode porosity [16], ε_0	0.88
Compressed electrode thickness, d_e	1.5×10^{-4} m
Compressed electrode porosity, ε	0.67
Average inter-fiber distance, δ	3.0×10^{-5} m
Pump efficiency, ψ_{pump}	0.9
Kozeny-Carmen Coefficient, k_{CK}	4.28
Total vanadium concentration, c_{total}	1700 mol·m^{-3}
Reference concentration, c^{ref}	1000 mol·m^{-3}
State of charge, SOC	0.5
Operation temperature, T	298 K
Positive reaction rate constant [42], k_{pos}	6.8×10^{-7} m·s^{-1}
Negative reaction rate constant [43], k_{neg}	1.7×10^{-7} m·s^{-1}
Diffusion coefficient of VO^{2+} [42], D_4	3.9×10^{-10} m^2·s^{-1}
Diffusion coefficient of VO_2^+ [42], D_5	3.9×10^{-10} m^2·s^{-1}
Diffusion coefficient of V^{2+} [42], D_2	2.4×10^{-10} m^2·s^{-1}
Diffusion coefficient of V^{3+} [42], D_3	2.4×10^{-10} m^2·s^{-1}
Positive equilibrium potential [19], E_{pos}^0	1.004 V
Negative equilibrium potential [19], E_{neg}^0	−0.255 V

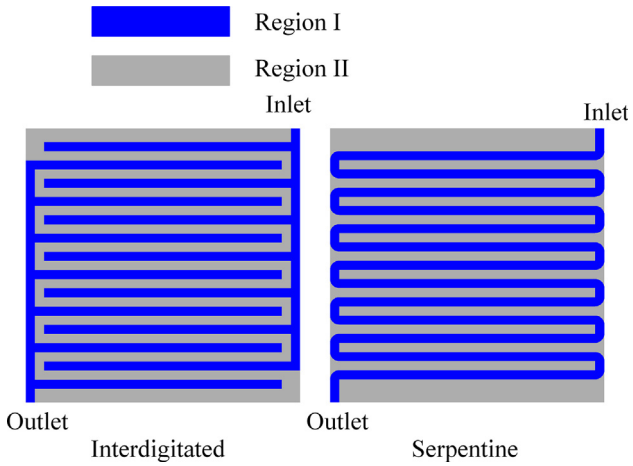

Fig. 2. Design of flow fields for model validation.

To demonstrate the effectiveness of our electrochemical reaction model, the iR-corrected overpotential is simulated as shown in Fig. 4. It is calculated through the overpotentials at negative and positive sides excluding the overpotential associated with electrical resistance. The results show that the simulated iR-corrected overpotential in the interdigitated flow field behaves higher than simulated value in serpentine flow field. This is in consistence with the experimental data as shown in Fig. 4(b), which is derived from Houser et al. [16]. The gap between the simulation and experimental data may be resulted from the estimated properties of porous electrodes.

3.2. Effect of flow field type on distribution uniformity

Uniformity factors are used to evaluate the distribution of local current density, indicating the uniformity of electrochemical reactions. As depicted in Fig. 5, the simulation with inlet electrolyte flow of 50% SOC show that interdigitated flow field demonstrates higher uniformity factor of current density than serpentine flow field in both negative and positive sides. Herein, the distribution of electrochemical reactions in interdigitated flow field is more uniform. This is in consistent with the experimental data by Houser et al. [16]. The uniformity factor of vanadium concentration in the interdigitated flow field design is higher than that in the serpentine design for both sides as shown in Fig. 6. Along with the increase in applied current density, the uniformity factor steps down and becomes much moderate at higher current densities. At relatively low current densities, vanadium conversions associated with electrochemical reactions are rather gentle along the electrolyte flow. However, the conversion rates of vanadium ions in the regions which is far from the inlet reach the maximum resulting from the reactants starvation at high current densities. Herein, electrochemical reaction rates are controlled by mass transport and vanadium concentrations are very low in these regions. With the increase of current densities, growing area in porous electrodes reaches the starvation region and the concentration distribution tends to be much uniform. As a result, the uniformity factor of VO_2^+ demonstrates moderate decrease at high current densities (see Fig. 6).

However, the uniformity factors of local current density and vanadium ions in a certain flow field for both negative and positive sides are similar. Therefore, the Fig. 7 only shows the distribution of overpotential, local current density and VO_2^+ vanadium ion at 100 mA/cm^2.

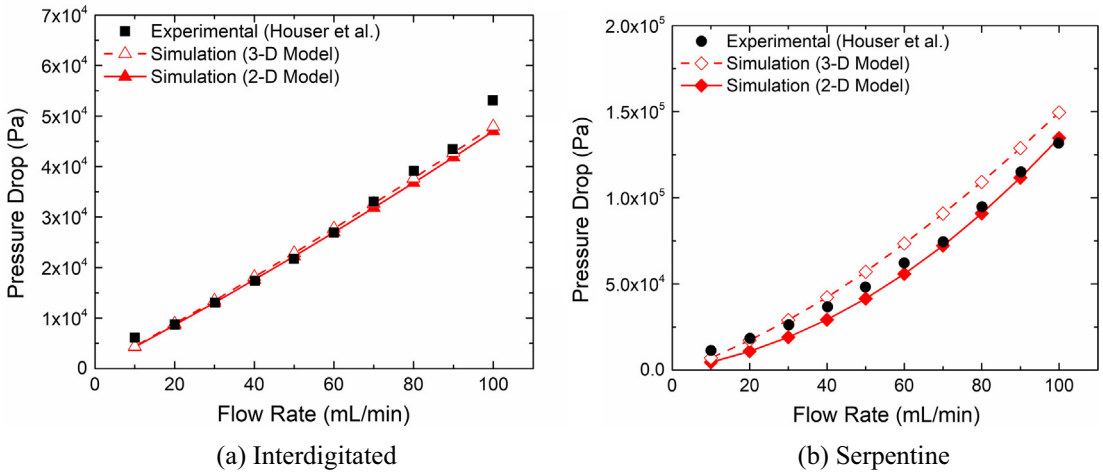

Fig. 3. Comparison of calculated and measured pressure drop.

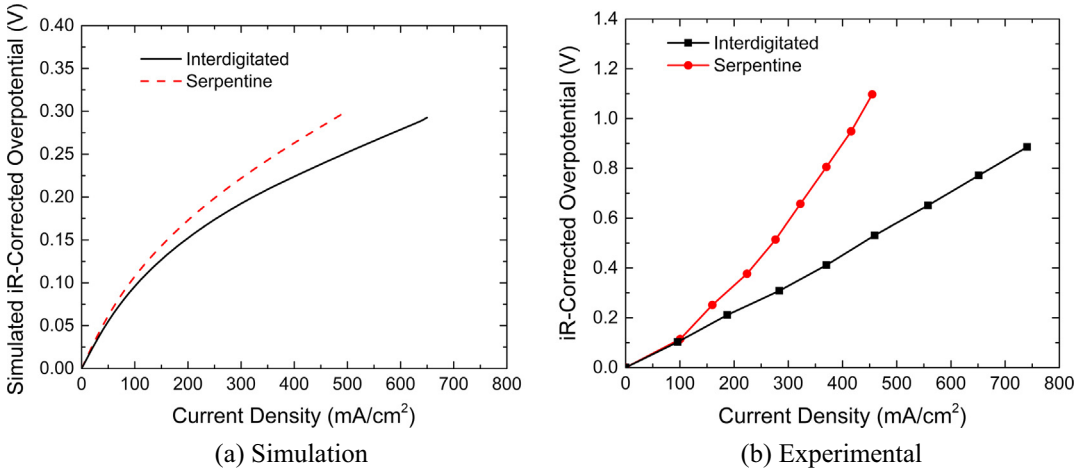

Fig. 4. Comparison of simulated iR-corrected overpotential with experimental data from [16].

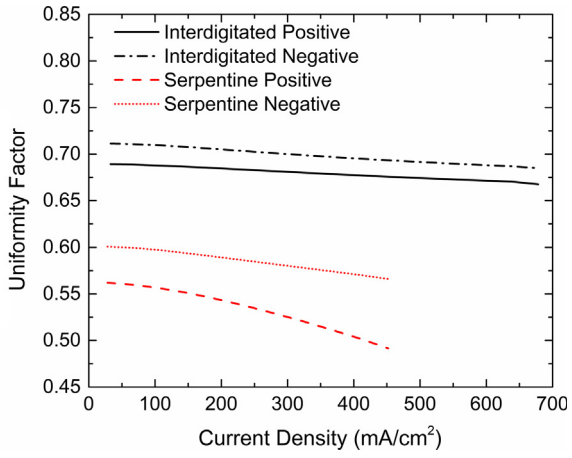

Fig. 5. Uniformity factor of local current density.

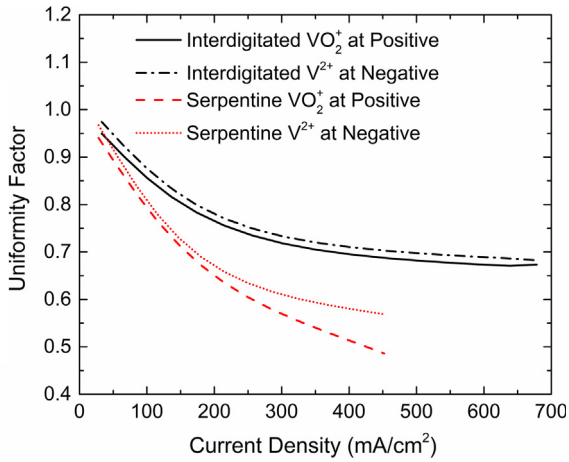

Fig. 6. Uniformity factor of vanadium ions at different current densities.

For different design of flow fields, the uniformity of reactions in porous electrodes is dramatically influenced by mass transport along with the electrolyte flow. In serpentine flow field design, electrolyte flow under the ribs of flow fields demonstrates very low flow velocity, resulting from relatively low permeability considering the open channels in serpentine flow field. With the interdigitated flow field design applied, the electrolyte is forced to flow through porous electrode under ribs. Thus, the flow velocity in porous electrode under ribs is much higher than serpentine design. Compared with serpentine flow field design, the electrolyte veloc-

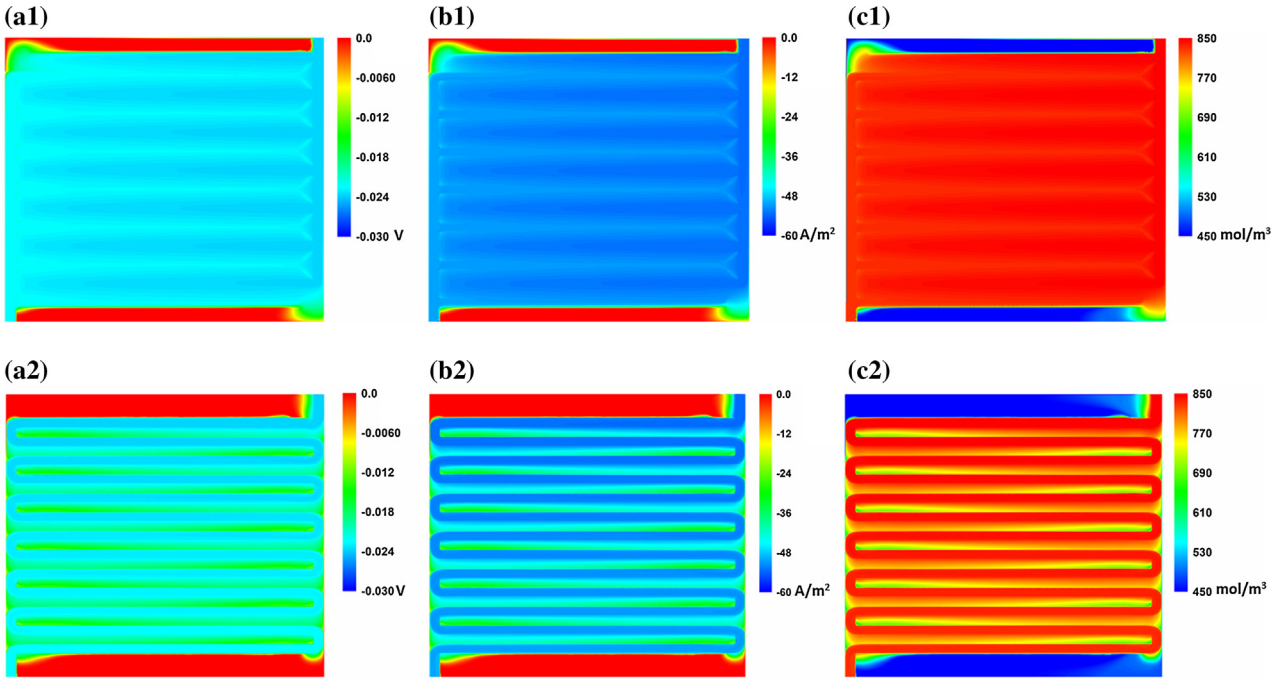

Fig. 7. Distribution of (a) overpotential, (b) local current density and (c) vanadium concentration for (1) interdigitated and (2) serpentine flow field.

ity in channels is much lower due to the increase of cross-sectional area. However, electrolyte flow path in interdigitated flow field design is much shorter than that in serpentine flow field design. More uniformity of overpotential and local current density in the interdigitated flow field in Fig. 7(a) and (b) reveals that shorter flow path dominates the mass transport and reactants flowing from inlet reach the carbon fiber surfaces in porous electrode more easily.

Concentration distributions of vanadium ions are determined by mass transport and electrochemical reactions. Vanadium reactants are transported through the electrolyte flow from the inlet of flow field. Electrochemical reactions occurred in these regions contribute to the consumption and generation of vanadium ions. Although the electrolyte flow velocity is relatively low in the interdigitated flow field design, electrolyte flow paths away from the inlet are much shorter than serpentine flow field design, determining higher mass transfer rate from inlet. This leads to the uniform distribution of VO_2^+ in the interdigitated flow field.

3.3. Design of flow fields in large active area cell

To apply our model in design of flow field for industrial scale stacks which are composed with large active area cells, appropriate channels should be designed to balance the distribution uniformity of vanadium ions required by excellent battery performance and pressure drop associated with the pumping power consumption. For an industrial scale flow battery system, the active area of cells is designed in the range of hundreds of square centimeters to meet the scale-up requirement of battery power. This feature usually enlarges the pressure drop significantly compared with lab-scale battery cell employing the similar flow field designs, thus increasing the pump power consumption consequently. Moreover, the mass transport in scale-up cells is influenced by electrolyte flow in channels and porous electrodes more remarkably. In this section, the active area of about 410-cm^2 was chosen as a typical case for the flow field design.

Interdigitated flow field design and serpentine design of flow fields with different number of parallel channels are shown in Fig. 8. The active area of cell is 410-cm^2. Channel height d_h and width d_w are both 2 mm. Parallel channel number $N_{channel}$ of serpentine design of flow fields is 1–5. The designs of flow field in this work contains interdigitated flow field and parallel serpentine flow fields which behave much different from flow field design of single serpentine channel. The Fig. 9 shows the pumping power derived from pressure drop in different design of flow fields. The calculation of pumping power includes two pumps, which is necessary for providing of negative and positive electrolyte at the same time. With two pump for negative and positive sides considered, the pumping power is calculated by:

$$P_{pump} = \frac{2\omega \cdot \Delta p}{\psi_{pump}} \tag{27}$$

where Δp is the pressure drop and ψ_{pump} is the pump efficiency.

For the serpentine design of flow fields, the pumping power reduces with the increasing in number of parallel serpentine channels. The parallel channels enhance the section area, thus decreasing the electrolyte flow velocities at a constant flow rate. The max cell power at the current density of 100 mA/cm^2 is also plotted in the figure for comparison. Compared to the max power, the flow field designs with one, two and three serpentine channels behave relatively very high pumping power. For a flow field design applied with four and five parallel serpentine channels, the pumping power decreases close to and even lower than that in the interdigitated design of flow field. The results demonstrate that the pumping power resulting from the pressure drop of the simulated architectures for the 410 cm^2 cell contribute to the power losses significantly for some designed architectures of flow fields.

The Fig. 10 shows the calculated results during discharge stage at 100 mA/cm^2 to evaluate the distribution uniformity in design of flow fields for large cell. The uniformity factor of current density in serpentine flow field design with three, four and five parallel channels is much lower than that of interdigitated design, indicating that the electrochemical reactions are much less uniform in serpentine designs with parallel channels. Therefore, number of channels need to be carefully designed for the application in VRFBs, balancing the pumping power and uniformity of electrochemical

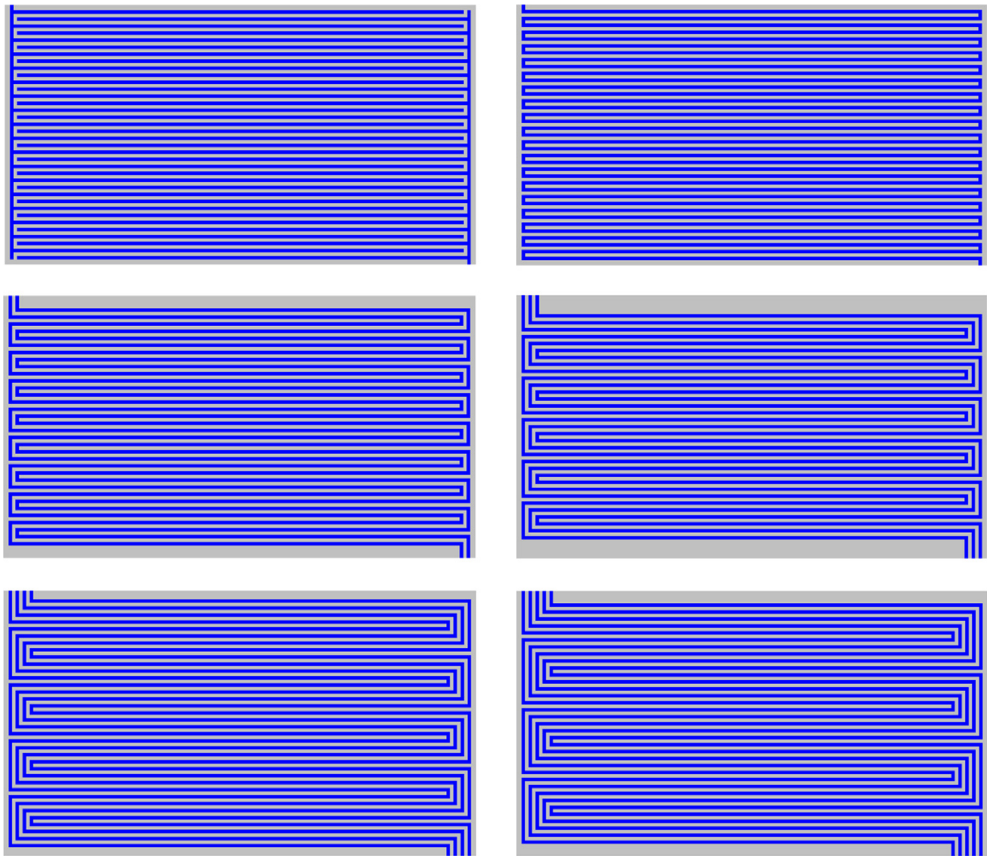

Fig. 8. Design of flow fields for the large cell.

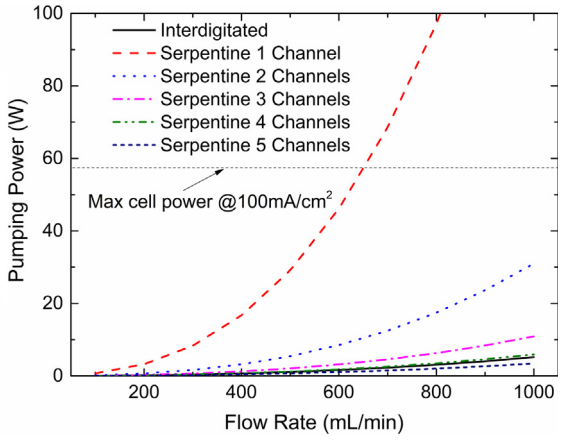

Fig. 9. Pumping power associated with pressure drop for different design of flow fields.

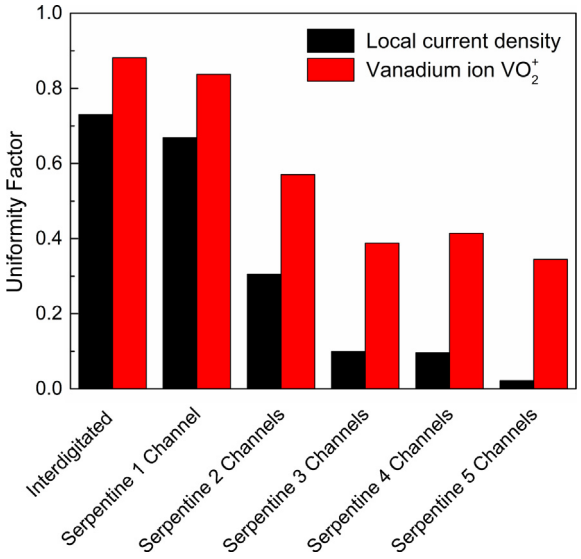

Fig. 10. Uniformity factors of local current density and vanadium ion concentration for the large active area cell.

reactions distribution. The results of the uniformity factor of VO_2^+ concentration during discharge stage show that the design of flow fields with parallel serpentine channels demonstrated less uniform distribution of vanadium ions. Serpentine design with more channels demonstrates much lower values indicating less uniformity. The results show that the interdigitated flow field design in this 410-cm^2 cell possesses comparatively low pumping power and much more uniform distribution in electrochemical reactions and reactants in electrochemical reactions.

The distribution of current density indicated the uniformity of electrochemical reactions in porous electrodes, and the distribution of vanadium ion concentration described the uniformity of mass transport in flow field and porous electrodes. The vanadium ions were transported along with the electrolyte flow from the inlet of battery cell. The simulation of electrolyte flow and mass transport coupled with electrochemical reaction in different design of flow fields proved the feasibility of developed model. With this model, the pumping power and mass transport uniformity in VRFBs could be sufficiently studied.

4. Conclusions

In summary, we reported a two-dimensional model for the flow field design of VRFBs. With the combination of momentum conservation, mass conservation and electrochemical kinetics, various flow field designs were studied to determine the pressure drop and distribution uniformity in VRFB cells. This model was validated through the comparison with experimental results. In this model, uniformity factors were utilized to evaluate the distribution uniformity of electrochemical reactions and vanadium ions which were served as reactants quantitatively. Investigation on the serpentine and interdigitated design of flow fields applied in this work indicated that lower pressure drop and more uniform in distribution of electrochemical reactions and reactants in the interdigitated flow field. The results were significantly influenced by the detailed design and specifications of flow fields.

To demonstrate the application capability of our flow field design model in modular stack, different design of flow fields for a larger active area of 410-cm^2 was numerically investigated. The results showed that the interdigitated flow field demonstrated nearly the lowest pumping power and highest distribution uniformity of electrochemical reactions and vanadium ions. With the increase in channel number for serpentine design, the pump power drop down while less distribution of vanadium ions comes up. Our developed model could do a lot to the design of flow fields for industrial-scale VRFB cells in ranges of active area.

Conflict of interest

The authors declare no interest of conflict.

Acknowledgments

This work was supported by the Open Projects of State Key Laboratory of Multiphase Flow in Power Engineering of China and a grant from the Research Grant Council of the Hong Kong Special Administrative Region, China (Project No. T23-601/17-R).

References

[1] M. Park, J. Ryu, W. Wang, J. Cho, Material design and engineering of next-generation flow-battery technologies, Nat. Rev. Mater. 2 (1) (2016).
[2] Q. Xu, T.S. Zhao, Fundamental models for flow batteries, Prog. Energy Combust. Sci. 49 (2015) 40–58.
[3] P. Leung, X. Li, C. Ponce de León, L. Berlouis, C.T.J. Low, F.C. Walsh, Progress in redox flow batteries, remaining challenges and their applications in energy storage, RSC Adv. 2 (27) (2012) 10125.
[4] X.L. Zhou, T.S. Zhao, L. An, Y.K. Zeng, X.H. Yan, A vanadium redox flow battery model incorporating the effect of ion concentrations on ion mobility, Appl. Energy 158 (2015) 157–166.
[5] Y. Lei, B.W. Zhang, B.F. Bai, T.S. Zhao, A transient electrochemical model incorporating the Donnan effect for all-vanadium redox flow batteries, J. Power Sources 299 (2015) 202–211.
[6] Y. Lei, B.W. Zhang, Z.H. Zhang, B.F. Bai, T.S. Zhao, An improved model of ion selective adsorption in membrane and its application in vanadium redox flow batteries, Appl. Energy 215 (2018) 591–601.
[7] C.W. Wong, T.S. Zhao, Q. Ye, J.G. Liu, Experimental investigations of the anode flow field of a micro direct methanol fuel cell, J. Power Sources 155 (2) (2006) 291–296.
[8] S.S. Hsieh, H.C. Wu, B.S. Her, A novel design for a flow field configuration, of a direct methanol fuel cell, J. Power Sources 195 (10) (2010) 3224–3230.
[9] C. Xu, T.S. Zhao, A new flow field design for polymer electrolyte-based fuel cells, Electrochem. Commun. 9 (3) (2007) 497–503.
[10] B.H. Lim, E.H. Majlan, W.R.W. Daud, M.I. Rosli, T. Husaini, Numerical analysis of modified parallel flow field designs for fuel cells, Int. J. Hydrogen Energy 42 (14) (2017) 9210–9218.
[11] Y.L. Wang, S.X. Wang, G.Z. Wang, L.K. Yue, Numerical study of a new cathode flow-field design with a sub-channel for a parallel flow-field polymer electrolyte membrane fuel cell, Int. J. Hydrogen Energy 43 (4) (2018) 2359–2368.
[12] A.P. Manso, F.F. Marzo, J. Barranco, X. Garikano, M.G. Mujika, Influence of geometric parameters of the flow fields on the performance of a PEM fuel cell. A review, Int. J. Hydrogen Energy 37 (20) (2012) 15256–15287.
[13] J.Y. Wang, Theory and practice of flow field designs for fuel cell scaling-up: a critical review, Appl. Energy 157 (2015) 640–663.
[14] D.S. Aaron, Q. Liu, Z. Tang, G.M. Grim, A.B. Papandrew, A. Turhan, T.A. Zawodzinski, M.M. Mench, Dramatic performance gains in vanadium redox flow batteries through modified cell architecture, J. Power Sources 206 (2012) 450–453.
[15] C.R. Dennison, E. Agar, B. Akuzum, E.C. Kumbur, Enhancing mass transport in redox flow batteries by tailoring flow field and electrode design, J. Electrochem. Soc. 163 (1) (2015) A5163–A5169.
[16] J. Houser, J. Clement, A. Pezeshki, M.M. Mench, Influence of architecture and material properties on vanadium redox flow battery performance, J. Power Sources 302 (2016) 369–377.
[17] J. Houser, A. Pezeshki, J.T. Clement, D. Aaron, M.M. Mench, Architecture for improved mass transport and system performance in redox flow batteries, J. Power Sources 351 (2017) 96–105.
[18] J. Marschewski, L. Brenner, N. Ebejer, P. Ruch, B. Michel, D. Poulikakos, 3D-printed fluidic networks for high-power-density heat-managing miniaturized redox flow batteries, Energy Environ. Sci. 10 (3) (2017) 780–787.
[19] A.A. Shah, M.J. Watt-Smith, F.C. Walsh, A dynamic performance model for redox-flow batteries involving soluble species, Electrochim. Acta 53 (27) (2008) 8087–8100.
[20] A.A. Shah, H. Al-Fetlawi, F.C. Walsh, Dynamic modelling of hydrogen evolution effects in the all-vanadium redox flow battery, Electrochim. Acta 55 (3) (2010) 1125–1139.
[21] H. Al-Fetlawi, A.A. Shah, F.C. Walsh, Modelling the effects of oxygen evolution in the all-vanadium redox flow battery, Electrochim. Acta 55 (9) (2010) 3192–3205.
[22] A. Shah, R. Tangirala, R. Singh, R.G.A. Wills, F.C. Walsh, A dynamic unit cell model for the all-vanadium flow battery, J. Electrochem. Soc. 158 (6) (2011) A671–A677.
[23] K.W. Knehr, E.C. Kumbur, Open circuit voltage of vanadium redox flow batteries: discrepancy between models and experiments, Electrochem. Commun. 13 (4) (2011) 342–345.
[24] K.W. Knehr, E. Agar, C.R. Dennison, A.R. Kalidindi, E.C. Kumbur, A transient vanadium flow battery model incorporating vanadium crossover and water transport through the membrane, J. Electrochem. Soc. 159 (9) (2012) A1446–A1459.
[25] D. You, H. Zhang, J. Chen, A simple model for the vanadium redox battery, Electrochim. Acta 54 (27) (2009) 6827–6836.
[26] D. You, H. Zhang, C. Sun, X. Ma, Simulation of the self-discharge process in vanadium redox flow battery, J. Power Sources 196 (3) (2011) 1578–1585.
[27] X. Ke, J.I.D. Alexander, J.M. Prahl, R.F. Savinell, Flow distribution and maximum current density studies in redox flow batteries with a single passage of the serpentine flow channel, J. Power Sources 270 (2014) 646–657.
[28] X. Ke, J.I.D. Alexander, J.M. Prahl, R.F. Savinell, A simple analytical model of coupled single flow channel over porous electrode in vanadium redox flow battery with serpentine flow channel, J. Power Sources 288 (2015) 308–313.
[29] X.Y. Ke, J.M. Prahl, J.I.D. Alexander, R.F. Savinell, Mathematical modeling of electrolyte flow in a segment of flow channel over porous electrode layered system in vanadium flow battery with flow field design, Electrochim. Acta 223 (2017) 124–134.
[30] X.Y. Ke, J.M. Prahl, J.I.D. Alexander, R.F. Savinell, Redox flow batteries with serpentine flow fields: distributions of electrolyte flow reactant penetration into the porous carbon electrodes and effects on performance, J. Power Sources 384 (2018) 295–302.
[31] Q. Ye, J. Hu, P. Cheng, Z. Ma, Design trade-offs among shunt current, pumping loss and compactness in the piping system of a multi-stack vanadium flow battery, J. Power Sources 296 (2015) 352–364.
[32] X. You, Q. Ye, P. Cheng, Scale-up of high power density redox flow batteries by introducing interdigitated flow fields, Int. Commun. Heat Mass Transfer 75 (2016) 7–12.
[33] Q. Xu, T.S. Zhao, P.K. Leung, Numerical investigations of flow field designs for vanadium redox flow batteries, Appl. Energy 105 (2013) 47–56.
[34] E. Knudsen, P. Albertus, K.T. Cho, A.Z. Weber, A. Kojic, Flow simulation and analysis of high-power flow batteries, J. Power Sources 299 (2015) 617–628.
[35] M. Messaggi, P. Canzi, R. Mereu, A. Baricci, F. Inzoli, A. Casalegno, M. Zago, Analysis of flow field design on vanadium redox flow battery performance: development of 3D computational fluid dynamic model and experimental validation, Appl. Energy 228 (2018) 1057–1070.
[36] J.T. Gostick, M.W. Fowler, M.D. Pritzker, M.A. Ioannidis, L.M. Behra, In-plane and through-plane gas permeability of carbon fiber electrode backing layers, J. Power Sources 162 (1) (2006) 228–238.
[37] G.A. Truskey, F. Yuan, D.F. Katz, Transport phenomena in biological systems, 2004.
[38] R. Carta, S. Palmas, A. Polcaro, G. Tola, Behaviour of a carbon felt flow by electrodes Part I: mass transfer characteristics, J. Appl. Electrochem. 21 (9) (1991) 793–798.
[39] A. Parasuraman, T.M. Lim, C. Menictas, M. Skyllas-Kazacos, Review of material research and development for vanadium redox flow battery applications, Electrochim. Acta 101 (2013) 27–40.

[40] Q. Ye, T.S. Zhao, C. Xu, The role of under-rib convection in mass transport of methanol through the serpentine flow field and its neighboring porous layer in a DMFC, Electrochim. Acta 51 (25) (2006) 5420–5429.
[41] R.K. Shah, A.L. London, Laminar Flow Forced Convection in Ducts: A Source Book for Compact Heat Exchanger Analytical Data, Academic press, 2014.
[42] T. Yamamura, N. Watanabe, T. Yano, Y. Shiokawa, Electron-transfer kinetics of Np^{3+}/Np^{4+}, NpO_2^+/NpO_2^{2+}, V^{2+}/V^{3+}, and VO^{2+}/VO_2^+ at carbon electrodes, J. Electrochem. Soc. 152 (4) (2005) A830–A836.
[43] E. Sum, M. Skyllas-Kazacos, A study of the V (II)/V (III) redox couple for redox flow cell applications, J. Power Sources 15 (2–3) (1985) 179–190.